

## 4.2 Classical Two-Beam Interferometers

### 4.2.1 Young's double-pinhole interferometer (YDPI)

The Young's double pinhole interferometer (YDPI) is an extremely useful tool in understanding many aspects of interference. The basic YDPI is shown in Fig. 4.27, where two pinholes in an otherwise opaque screen effectively create two expanding spherical waves S1 and S2 that interfere to produce hyperboloidal fringe centers in the observation plane, as described by Eq. (4.42). When illuminated with a point source on axis or with an on-axis plane wave, S1 and S2 vibrate in phase. Hole size must be small relative to observation distance  $z_0$  and pinhole separation  $d$  in order to produce effects of spherical waves in transmission. Typically, effects of interest are centered around the  $y$  axis at large  $z_0$ , where straight-line, equally spaced cosine fringes are observed with OPD given by Eq. (4.45).

### 4.2.2 Young's double slit interferometer (YDSI)

The Young's double slit interferometer (YDSI) is similar to the YDPI. Instead of two pinholes, two parallel slits are oriented in the aperture plane separated by distance  $d$ . When the slits are oriented parallel to the  $x$  axis, the YDSI profile is identical to Fig. 4.27. Instead of two spherical waves, two cylindrical waves are generated upon transmission through the slits. Fringe centers are described by Eq. (4.69), which is identical to Eq. (4.45) with  $x = 0$ . The YDSI has higher transmission than the YDPI, but it exhibits many of the same characteristics. Straight-line equally spaced cosine fringes are observed around the  $y$  axis at large  $y_0$ .

A vector electromagnetic simulation to a plane wave illuminating two slits in an aluminum plate is shown in Fig. 4.28. This realistic result clearly shows hyperbola-shaped fringes away from the aperture plane, but irradiance differs significantly from two-cylindrical wave interference when observed in proximity to the slits.

### 4.2.3 Lloyd's mirror

A simple mirror can be used as an interferometer if illuminated with an expanding spherical wave, like that from an ideal point source. For example, the Lloyd's mirror interferometer produces a virtual image of a point source, which is located as far below the mirror surface as the real source is above it, as shown in Fig. 4.29. Interference between the real and the virtual sources creates hyperboloidal fringes of revolution in the observation space to the right of the source plane, in which fringe centers are described by Eq. (4.42). One important difference in the fringe pattern is that the central fringe is dark, instead of bright, if there is a phase change in reflection off the mirror. Therefore, Eq. (4.42) describes dark fringe centers. Lloyd's mirror with a single point source is similar to the YDPI, in that a hyperboloidal field is generated from two-point-source interference, except for the fringe contrast reversal. Straight-line cosine fringes are observed near the optical axis in the observation plane with period given by Eq. (4.46).

#### 4.2.4 Fresnel's mirrors

Fresnel's mirrors are similar to Lloyd's mirror, except a second mirror is used to create a second virtual source, as shown in Fig. 4.30. The two virtual sources form hyperboloidal fringes of revolution, where bright fringe centers are described by Eq. (4.42). Light from the real point source is blocked from the observation plane. Orientation of the symmetry line is adjustable by positioning the mirrors.

#### 4.2.5 Fresnel's biprism

Yet another variation is Fresnel's biprism, as shown in Fig. 4.31, where two virtual point images  $S_1$  and  $S_2$  of source  $S$  are produced by an offset pair of prisms with refractive index  $n$ . If the reflections from the prism faces are negligible, then the two virtual point images, one from each prism, produce an interference pattern in much the same way as the YDPI. The distance  $z_0$  in Eq. (4.42) is measured from the virtual source plane, which is a distance  $nl$  behind the prisms.

#### 4.2.6 Plane parallel plate (PPP) interferometer

Perhaps the simplest form of interferometer is the plane parallel plate, as shown in Fig. 4.32. Light from point source  $S$ , which is a distance  $l$  in front of the plate, reflects from the two surfaces of the plate. The reflection from the front surface appears to originate from virtual source point  $S_1$  a distance  $l$  behind the plate. Part of the wave refracts into the plate and reflects off the back surface. When this wave exits the plate from the front, it appears to originate from virtual source point  $S_2$ . The coherent point-source pair  $S_1$  and  $S_2$  that are produced by the reflections are separated by the geometrical distance  $d = 2t/n$ . They have a symmetry line through  $S_1S_2$  perpendicular to the surface of the plate, and they produce a hyperboloidal fringe field that can be viewed from the front of the plate. (For practical experiments, the point source is isolated from the observation region with a beamsplitter or other component.) The glass causes an additional delay between the two waves that must be considered if the source is not monochromatic. Notice that the symmetry line is perpendicular to the plate's surface, and the  $m = 0$  fringe is parallel to the plate's surface.

Now consider a quasimonochromatic incoherent extended source, where each point on the source is an independent radiator that does not interfere with its neighbor. The quasimonochromatic characteristic implies that wavelength differences between the sources are insignificant over the range of observation. The PPP produces a reflection of each source point for each surface of the plate, as shown in Fig. 4.33 for point sources  $a$  and  $b$  at extreme ends of the source. (Realize that the source is composed of an infinite number of point sources between  $a$  and  $b$ .) Each virtual source pair produces a hyperboloidal fringe pattern in observation space. The individual fringe patterns are offset in the vertical direction according to the position of the point of origin in the source. The fringe patterns add in irradiance to produce the total light pattern. If the source length is greater than the fringe spacing, the hyperboloidal features wash out, and zero visibility is measured in observation region close to the plate.

In the particular geometry of Fig. 4.33, a useful characteristic of the fringe patterns is that asymptotes for each fringe order  $m$  are parallel. This condition exists because the virtual images of the source,  $a_1b_1$  and  $a_2b_2$ , are parallel to each other. If the observation plane is displaced far enough to the right of the plate so that the distance between adjacent fringe orders is larger than the length of the source, fringes with acceptable visibility can be measured. A practical way of achieving a long effective distance between the source pairs and the observation plane is to use a lens positioned as shown in Fig. 4.34, where the Observation plane is at the back focus of a lens. In this configuration, the image of the observation plane is at infinity with respect to the plate. Each fringe order at angle focuses to a circle in the observation plane, due to the symmetry of the hyperboloidal fringe field. The radius of the circle is given by  $r_m = f \cot\theta_m$ . The combination of all circles yields a concentric fringe pattern. Like with two-point-source interference, the maximum OPD of this pattern corresponds to the innermost fringe at the center of the circular pattern. Any significant width of the source power spectrum washes out the fringe in this central region, due to temporal coherence effects. The circular fringes shown in Fig. 4.34 are called *Haidinger's fringes*. Because the fringes are only observed at a sufficiently large distance from the plate, the fringes are said to be *localized at infinity*. Since each fringe results from many source points, but only from a specific angular range, the fringes are also called *fringes of equal inclination*.

#### 4.2.7 Fizeau interferometer and Newton's rings

Now consider interference formed by the two flat surfaces of a thin, wedged film. The wedge under test is very thin with respect to the distance from the source to the top surface. Effectively, the wedge is a *thin film*. In addition, the wedge angle is small. Figure 4.35 shows the geometry for a thin film illuminated by an extended incoherent quasimonochromatic source. In this case, the coherent pairs form hyperboloidal fringe fields, like those shown in the magnified view of the  $a_1a_2$  source pair. The  $m_a = 0$  fringe line is directed toward the film, where the  $m_b = 0$  fringe intersects with it. A similar observation is made concerning all other fringe orders. That is, like fringe orders intersect at or near the film, which produces high-contrast fringes. Between the source images and the film, the fringes are overlapped in various ways, and the fringe visibility is low or zero. Likewise, visibility is low beyond the film. Therefore, the fringes are *localized at the thin film*.

Figure 4.36 shows the result of a simulation for the geometry of Fig. 4.35 with film thickness  $t = 1\mu\text{m}$ , wedge angle  $= 0.1^\circ$ , wavelength  $= 500\text{nm}$ , plate refractive index  $n = 1.5$ ,  $l = 200\text{mm}$ , and separation between source points  $a$  and  $b$  of  $10\text{mm}$ . The fringe fields from coherent pairs are tilted and displaced with respect to each other. However, the fringe fields converge with like orders overlapping at the wedge. That is, the  $m^{\text{th}}$  order of the fringe field from source pair  $a_1a_2$  overlaps the  $m^{\text{th}}$  order of the fringe field from all other source pairs distributed along the images. Therefore, the visibility is maximum at the wedge and the fringes are localized at the thin film. An external optical system or the eye of an observer can be used to reimaged the wedge in order to detect high visibility

fringes. Notice that the  $m = 0$  fringe of each coherent pair intersects the wedge. Therefore, high visibility is obtained near the intersection of the  $m = 0$  fringe and the film wedge, even with a broad bandwidth light source. Also, the fringe pattern consists of straight-line, equally spaced fringes near the  $m = 0$  fringe, like what is observed in the two expanding spherical wave fringe pattern shown in Fig. 4.17 with  $z_0$  sufficiently large. Over a wider expanse of fringe orders, the *localization surface* is a sphere with diameter  $l$ . If the wedge is not a simple linear function, the fringes are not distributed in straight, equally spaced lines.

The practical geometry in Fig. 4.37 is a *Fizeau interferometer*, where an air-film wedge is formed between a test piece and a reference flat. Light from the extended source is blocked from directly reaching the observation plane by a beam splitter. For most of the test surface, the wedge is linear and fringes are straight and equally spaced. In the region of the bump, fringes move to positions of equal OPD, which are toward the open side of the wedge. The otherwise straight fringe lines are distorted in a shape characteristic of the bump.

The OPD between real-ray reflections from wedge surfaces can be used to find locations of bright and dark fringes along the film wedge. An additional factor from the phase difference  $\phi$  of the surface reflections must also be taken into account. For example, if an air wedge is sandwiched between two glass plates,  $\phi = \pi$ . When

$$\text{OPD} = m\lambda - \frac{\phi\lambda}{2\pi}, \quad (4.72)$$

a bright fringe is observed, and when

$$\text{OPD} = \left(m + \frac{1}{2}\right)\lambda - \frac{\phi\lambda}{2\pi}, \quad (4.73)$$

a dark fringe is observed. Since all like fringe orders overlap at the film, as shown in Fig. 4.36, it is sufficient to analyze the ray emitted from the central portion of the source. Derivation of OPD is aided by the magnified view of the wedge shown in Fig. 4.38, where real-ray path portions  $\overline{AB}$ ,  $\overline{CB}$  and  $\overline{AD}$  are to be determined and  $n_1$  is the refractive index of the incident medium,  $n_2$  is the refractive index of the wedge,  $t(x)$  is the thickness of the plate at the point of reflection, and  $\theta_2$  is the angle of refraction inside the wedge. OPD is

$$\begin{aligned}
\text{OPD} &= n_2 (\overline{AB} + \overline{CB}) - n_1 \overline{AD} \\
&= n_2 \frac{2t(x)}{\cos \theta_2} - n_1 \overline{AC} \sin \theta_1 \\
&= n_2 \frac{2t(x)}{\cos \theta_2} - n_1 2t(x) \tan \theta_2 \sin \theta_1 \\
&= 2n_2 t(x) \cos \theta_2 .
\end{aligned} \tag{4.74}$$

Notice that OPD in Eq. (4.74) is directly proportional to the thickness of the wedge  $t(x)$ . Therefore, fringes map out contours of constant wedge thickness. These fringes are called *fringes of equal thickness*.

For the case of nearly normal incidence ( $\theta \sim 0$ ) and  $n = 1$ ,  $\text{OPD} = 2t(x)$ , and each fringe represents one-half wavelength multiples of surface departure. For the bump shown in Fig. 4.37, the height of the defect is approximately the fractional fringe deviation  $\Delta/\Lambda$  multiplied by the surface departure between fringe lines. That is, *bump height* =  $(\lambda/2)(\Delta/\Lambda)$ .

In order to see the fringes, the wedge is imaged onto an observation plane. (Fringes can be imaged through optical systems, just like light reflected from or transmitted through real objects.) In a practical experiment, the observation plane can be a CCD array. The lens and observation plane can also be the eye and retina, respectively, of the observer if the fringes are viewed directly. Notice that localization of the fringes at the wedge is an advantage to the observer. Spurious fringes caused by reflections from other surfaces typically have very low visibility and do not distract from the measurement of interest. A Fizeau test of two flat plates is shown in Fig. 4.39.

The analysis outlined in Fig. 4.37 can be extended to transmitted fringes, where the OPD is defined by Eq. (4.72). However, phase shift  $\phi$  must be recalculated, due to the extra reflection. With a simple air wedge between two glass plates, visibility of transmitted fringes is much lower than the reflected fringes, due to the higher transmission of the first beam.

Naturally occurring thin films, like soap bubbles and oil films, produce colorful interference effects. In this case, constructive interference for different wavelengths is spread out spatially from small changes in  $t$  or  $\theta$ . An example of colored fringes from a soap bubble is shown in Fig. 4.40. This same concept can be applied to testing shallow etch patterns in optical element, like the spherical aberration compensators shown in Fig. 4.41. Different etch depths, which produce different phase shifts on transmission, display different colors in the Fizeau film under white-light illumination.

Newton's rings are a special type of Fizeau interference pattern formed by a circularly-symmetric quadratic wedge, as shown in Fig. 4.42. For example, if a flat plate and a spherical surface with radius  $R$  come in contact, thickness of the wedge is given by

$$t(x, y) \approx \frac{x^2 + y^2}{2R}, \quad (4.75)$$

when radius  $R$  is large. Lines of constant OPD form circular fringes. The value of  $|\text{OPD}|$  is minimum in the center of the pattern, so changes in source wavelength do not affect the center as much as the higher-order fringes at larger radii. In fact, white-light fringes are easily observed with Newton's Rings, as displayed in Fig. 4.42. Colored rings can be observed as radii increases. This phenomenon is not observable with Haidinger's fringes, even though they look similar, because  $|\text{OPD}|$  is maximum in the center of the Haidinger pattern.

#### 4.2.8 Twyman-Green interferometer

A Twyman-Green interferometer is sketched in Fig. 4.43. Collimated laser beam  $U(\mathbf{r}, t)$  illuminates both the flat reference mirror M1 and the test mirror M2 after beam splitter reflection and transmission, respectively. Path length from the beam splitter to the reference mirror is  $d_1$ , and path length from the beam splitter to the test mirror is  $d_2$ . Upon reflection from the test mirror, test beam phase is modified, due to surface height  $\varepsilon(x_0, y_0)$ . Observation space begins as soon as the beams reflected from each mirror combine after the beam splitter. OPD difference given by

$$\text{OPD}(x_0, y_0) = 2(d_1 - d_2) - 2\varepsilon(x_0, y_0). \quad (4.76)$$

With  $\phi$  as the phase difference of reflection from the two mirrors, bright fringes are observed when OPD satisfies Eq. (4.72). A Twyman-Green interferometer is called a *double-pass interferometer*, because the test beam OPD is modified by twice the surface departure  $\varepsilon(x_0, y_0)$ .<sup>5</sup> An interferogram made by using a Twyman-Green interferometer to test a spherical mirror is shown in Fig. 4.44. One fringe deviation represents  $\frac{1}{2}$  wave of surface departure, due to the double-pass nature of this interferometer.

#### 4.2.9 Mach-Zehnder interferometer

#### 4.2.10 Michelson interferometer

#### 4.2.11 Lateral shearing interferometer (LSI)

#### 4.2.12 Radial shearing interferometer (RSI)

#### 4.2.13 Polarization splitters

---

<sup>5</sup> Notice that the Fizeau interferometer, shown in Fig. 4.37, is also a double-pass interferometer.

4.2.14 Diffraction gratings

4.3 Multiple-Beam Interference

4.3.1 Airy's formula

4.3.2 Absorbing coatings

4.3.3 Fabret Perot (plane and spherical)

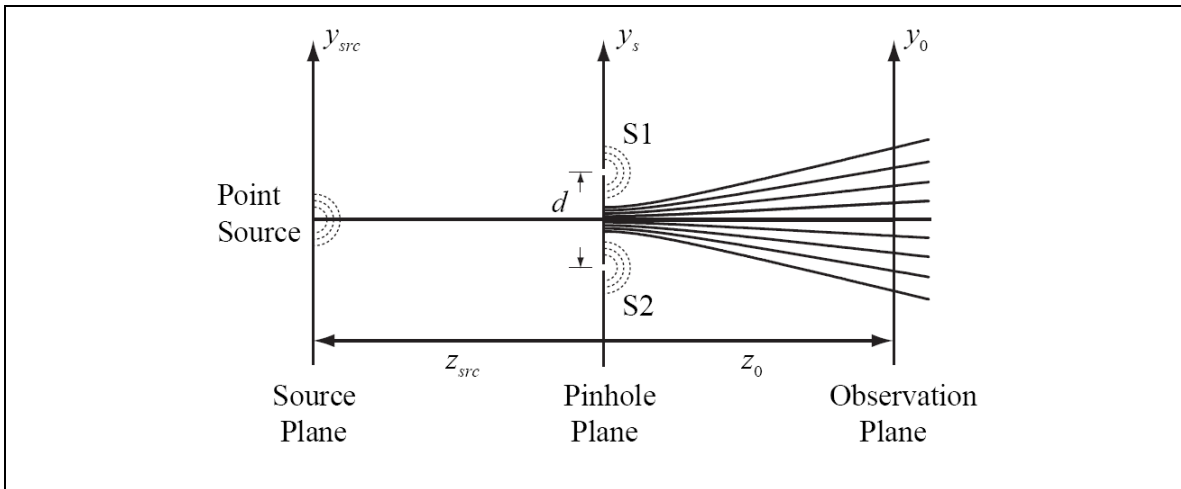


Figure 4.27. Basic Young's Double Pinhole Interferometer (YDPI). Two small holes in an otherwise opaque plate create two expanding spherical waves in transmission. Hyperboloidal fringes of revolution are formed in the observation space on the right side of the pinhole plane. This diagram also represents a Young's double slit interferometer (YDSI) when the slits are parallel to the  $x$  axis. The YDSI forms hyperbolas in  $yz$  planes of the observation space.

Figure 4.28.

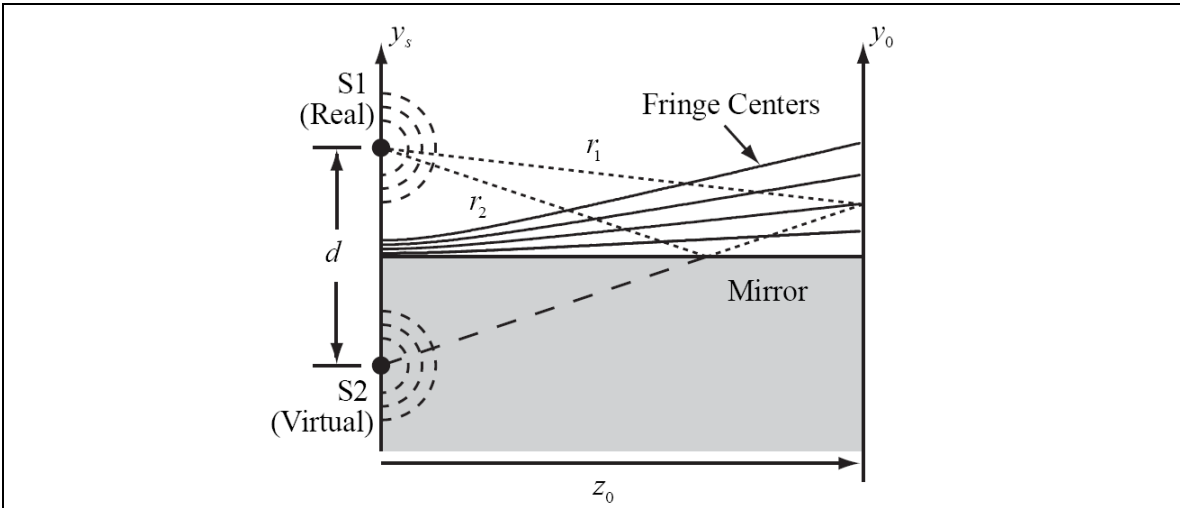


Figure 4.29. Basic Lloyd's Mirror Interferometer. A single reflection from a flat mirror produces a virtual expanding spherical wave S2 that interferes with the expanding spherical wave from the real source S1.

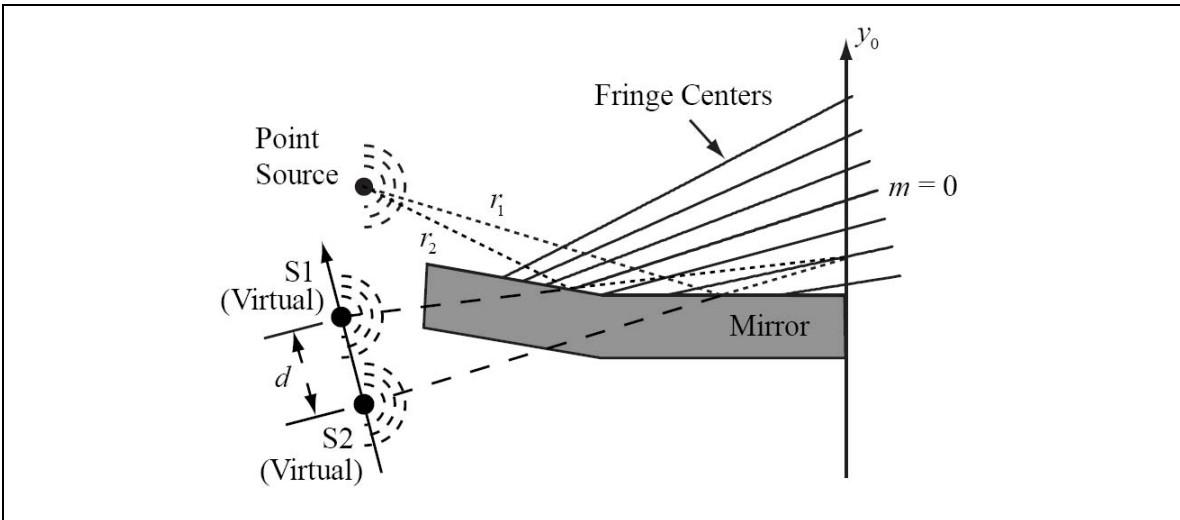


Figure 4.30. Fresnel's Mirrors. Two reflections from flat mirrors produce two virtual expanding spherical waves S1 and S2 and hyperboloidal fringes of revolution with an adjustable symmetry line.

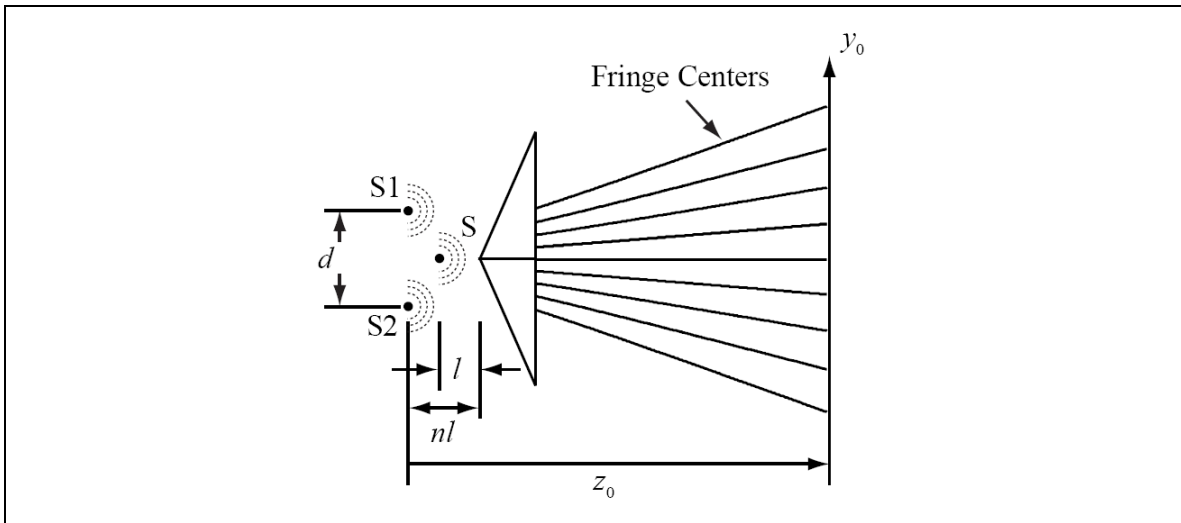


Figure 4.31. Fresnel's Biprism. Two offset prisms of index  $n$  form point images of source  $S$  a distance  $nl$  behind the prisms, where  $l$  is the distance from source  $S$  to the prisms. A hyperboloidal fringe field is generated in the observation space on the right side of the prisms.

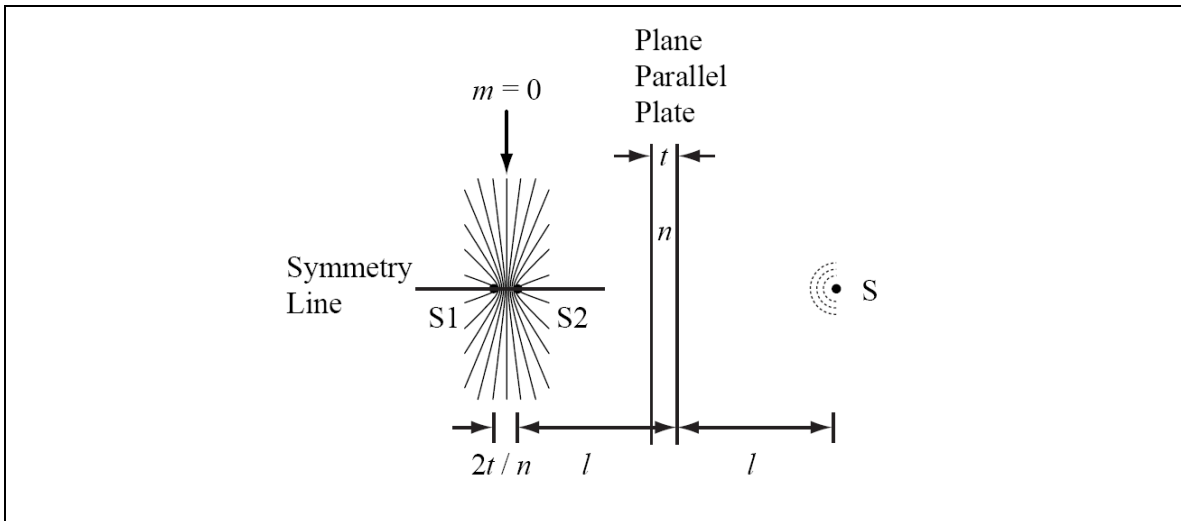


Figure 4.32 Plane Parallel Plate (PPP). Point source  $S$  is shown positioned a distance  $l$  in front of a PPP. A coherent pair of virtual point sources  $S1S2$  is created from the two Fresnel surface reflections of the plate. The coherent point-source pair produces a hyperboloidal fringe field in the observation space to the right of the plate.

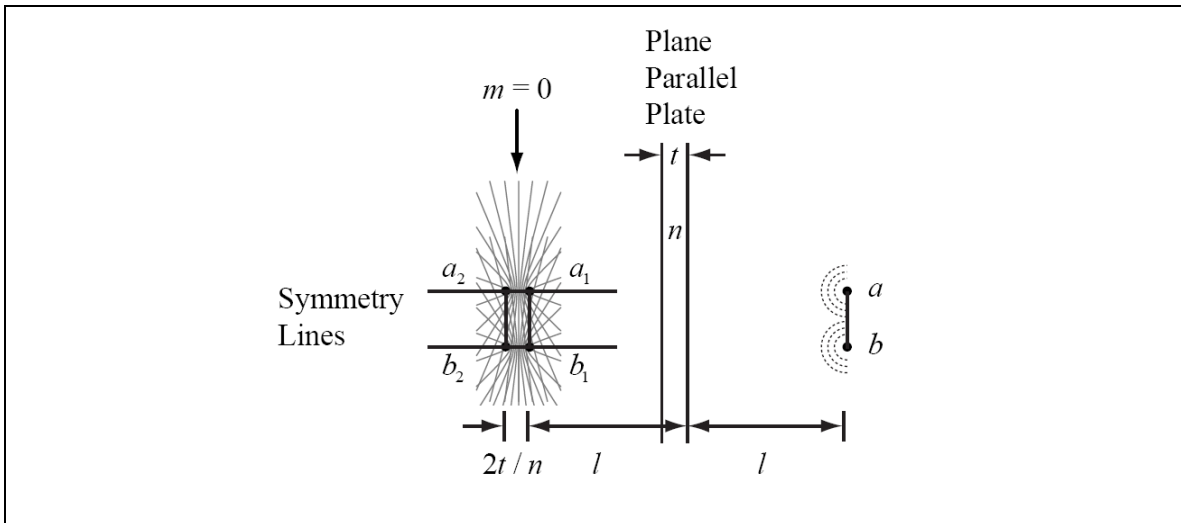


Figure 4.33 Plane Parallel Plate with an incoherent quasimonochromatic extended source. Extended source  $ab$  is shown positioned a distance  $l$  in front of a plane parallel plate (PPP). A coherent pair of virtual point sources is created for each point in the extended source from the two Fresnel surface reflections of the plate. Each coherent point-source pair produces a hyperboloidal fringe field in the observation space. The hyperboloids are shifted with respect to each other according to the source-point position. A reduction in visibility is observed in the observation space, due to overlap of the fringes.

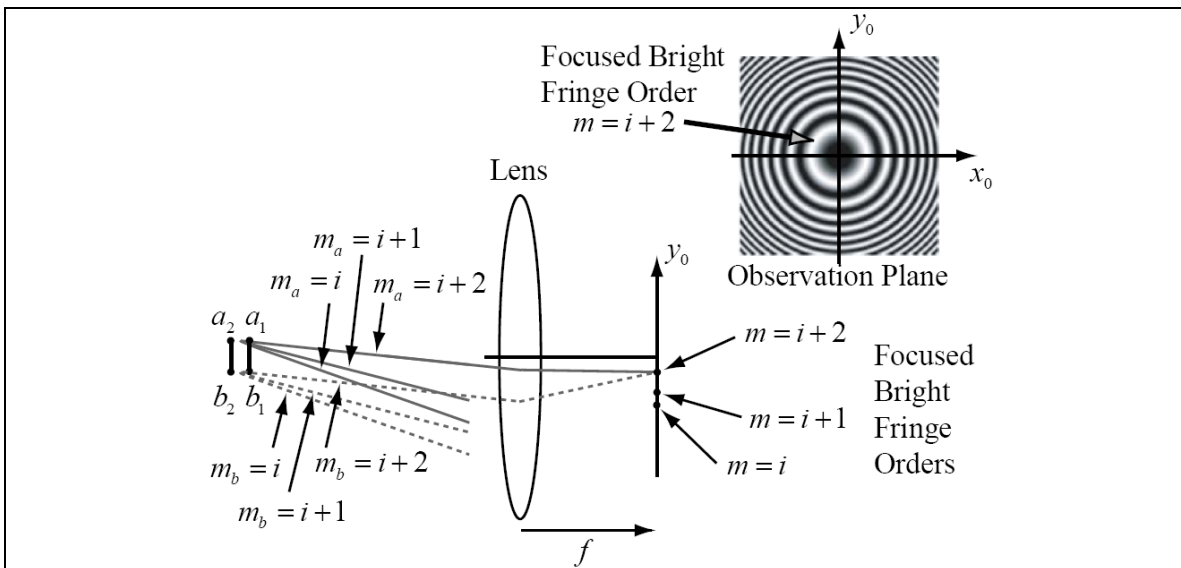


Figure 4.34. Haidinger's fringes. *Haidinger's fringes* or *fringes of equal inclination* are formed when images of the extended source are parallel to each other in observation space. Although fringes have low visibility near the source images, a lens with focal length  $f$  can be used to form the characteristic concentric-ring fringe pattern with good visibility. The pattern forms because fringe asymptotes of corresponding fringe orders are parallel. Since the lens effectively sets the observation at an infinite conjugate with respect to the source images, the fringes are said to be *localized at infinity*.

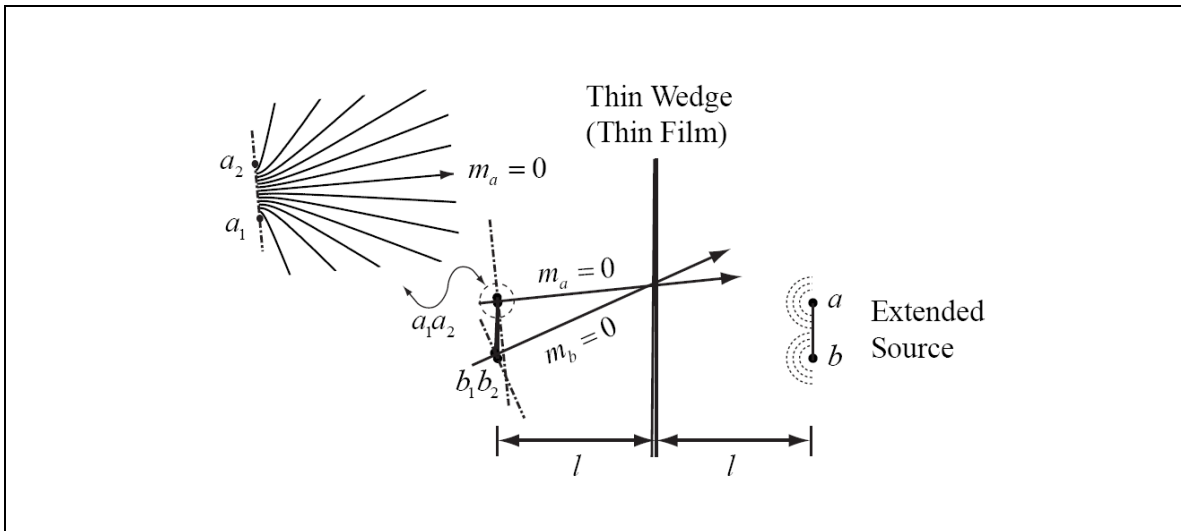


Figure 4.35. Thin wedge (thin film) with incoherent quasimonochromatic extended-source illumination. The extended source is positioned a distance  $l$  to the right of a thin film. A coherent pair of virtual point sources is created for each point in the source from the two Fresnel flat surface reflections of the film. Each coherent point-source pair produces a hyperboloidal fringe field in the observation space to the right of the film. Like orders intersect at the film, so the fringes are *localized at the thin film*.

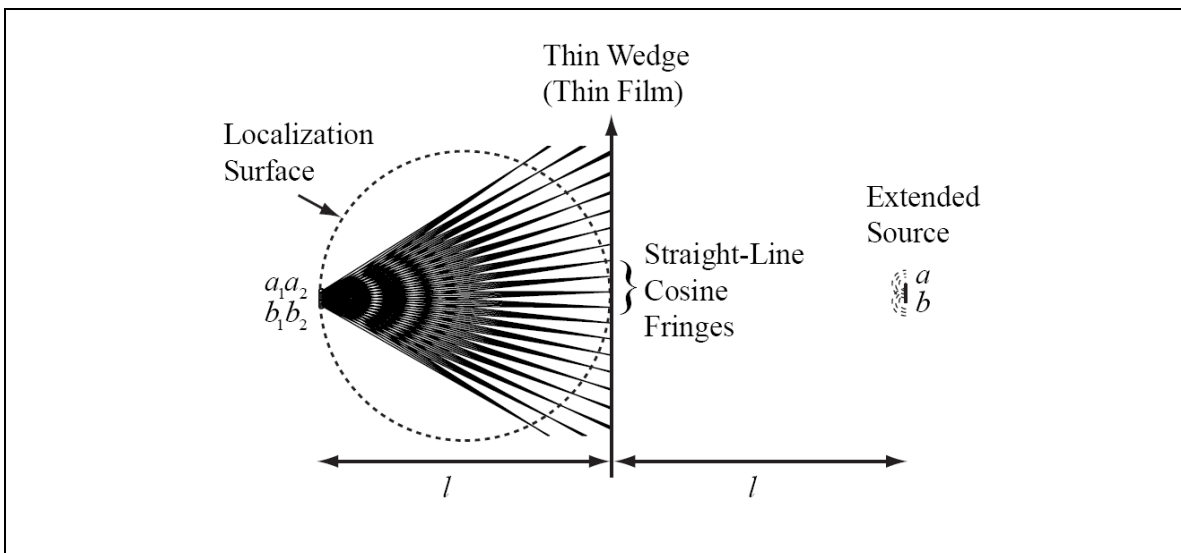


Figure 4.36. Result of a simulation for the geometry of Fig. 4.35 with film thickness  $t = 1\mu\text{m}$ , wedge angle  $= 0.1^\circ$ , wavelength  $= 500\text{nm}$ , plate refractive index  $n = 1.5$ ,  $l = 200\text{mm}$ , and separation between source points  $a$  and  $b$  of  $10\text{mm}$ .

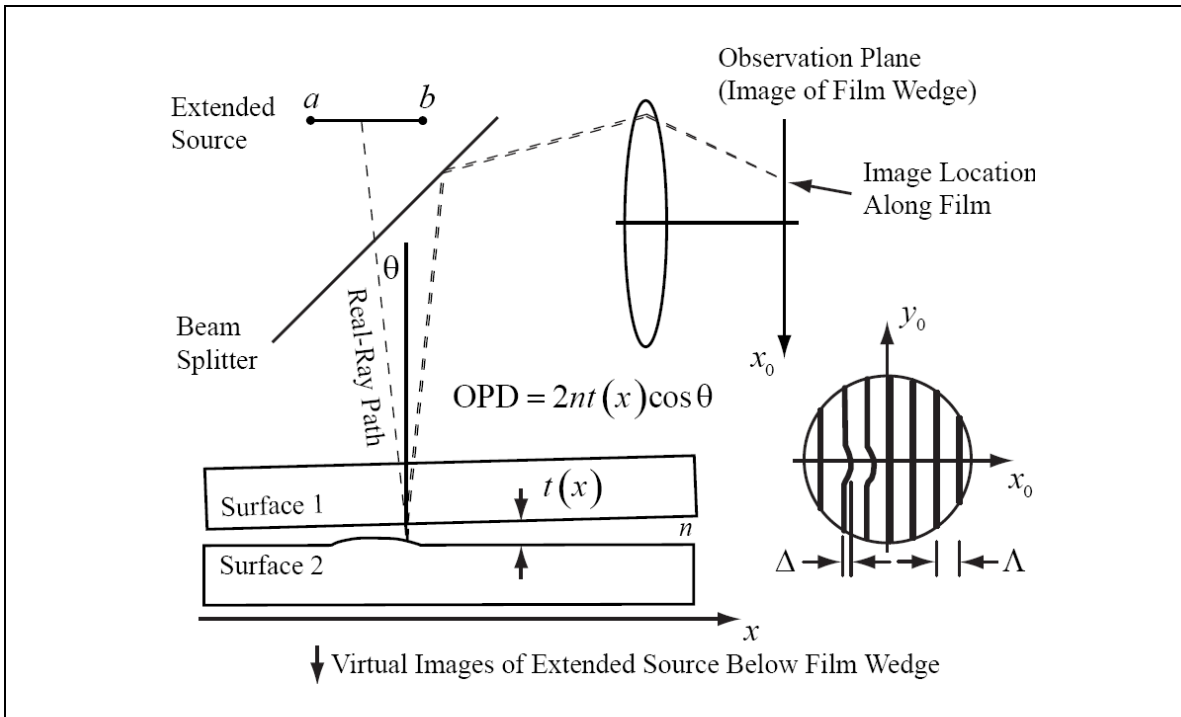


Figure 4.37. A typical Fizeau interferometer. Fringes of equal thickness indicate contours of constant  $t(x)$  and are localized at the wedge. The height of the defect, as indicated by the fringe deviation, is approximately  $\frac{\lambda\Delta}{2\Lambda}$ .

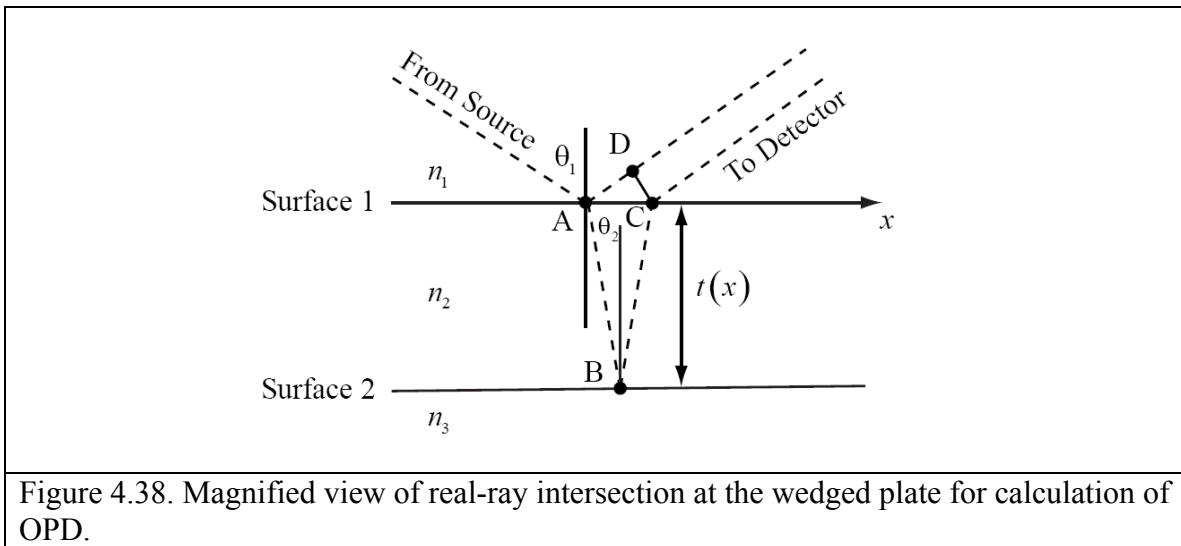


Figure 4.38. Magnified view of real-ray intersection at the wedged plate for calculation of OPD.

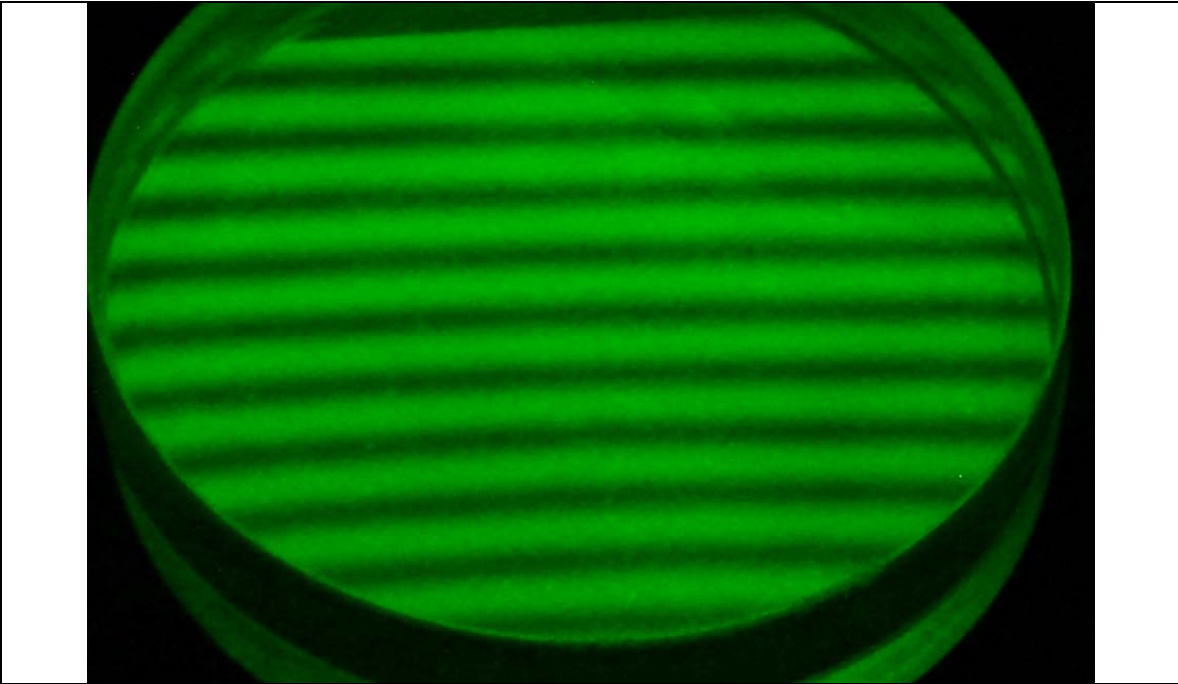


Figure 4.39. Fizeau fringes from two flat plates. Fringes are straight and equally spaced. An extended Hg lamp filtered for green transmission is used for illumination.

Figure 4.40. Colored fringes from a soap bubble.

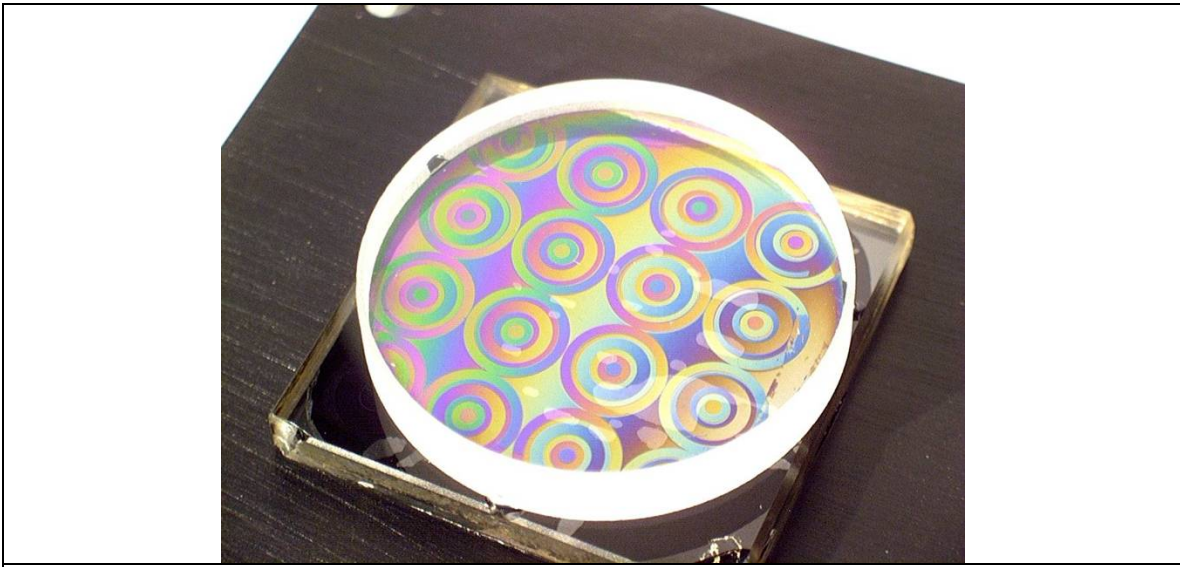


Figure 4.41. Example of a Fizeau film for testing spherical aberration compensators. Different etch thicknesses in the compensator plate show as different colors in the Fizeau film. A round optical flat is placed on top of the square compensator plate to form the Fizeau film. The Fizeau is illuminated with simple fluorescent white lights.

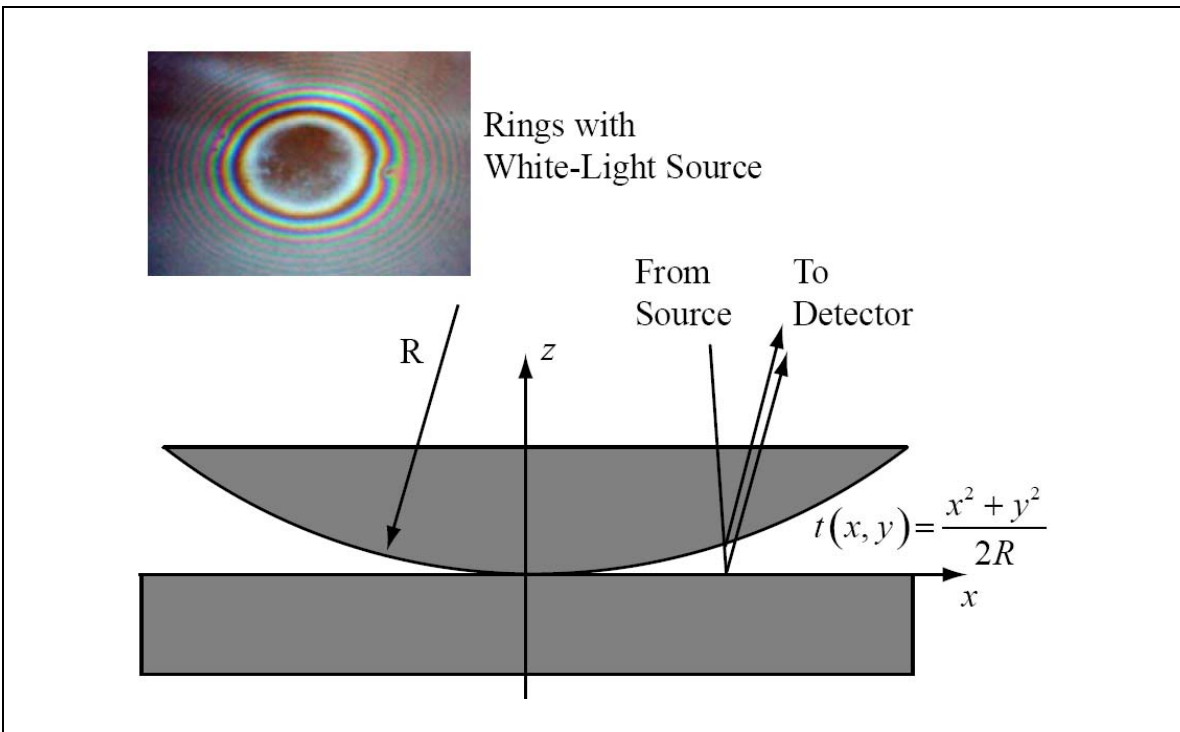


Figure 4.42. Newton's Rings. A quadratic film wedge produces circular fringes.  $|\text{OPD}|_{\text{min}}$  is in the center of the fringe pattern, unlike with Haidinger's fringes. With a white-light source, fringes exhibit highest visibility in the center and decrease in visibility with increasing radius.

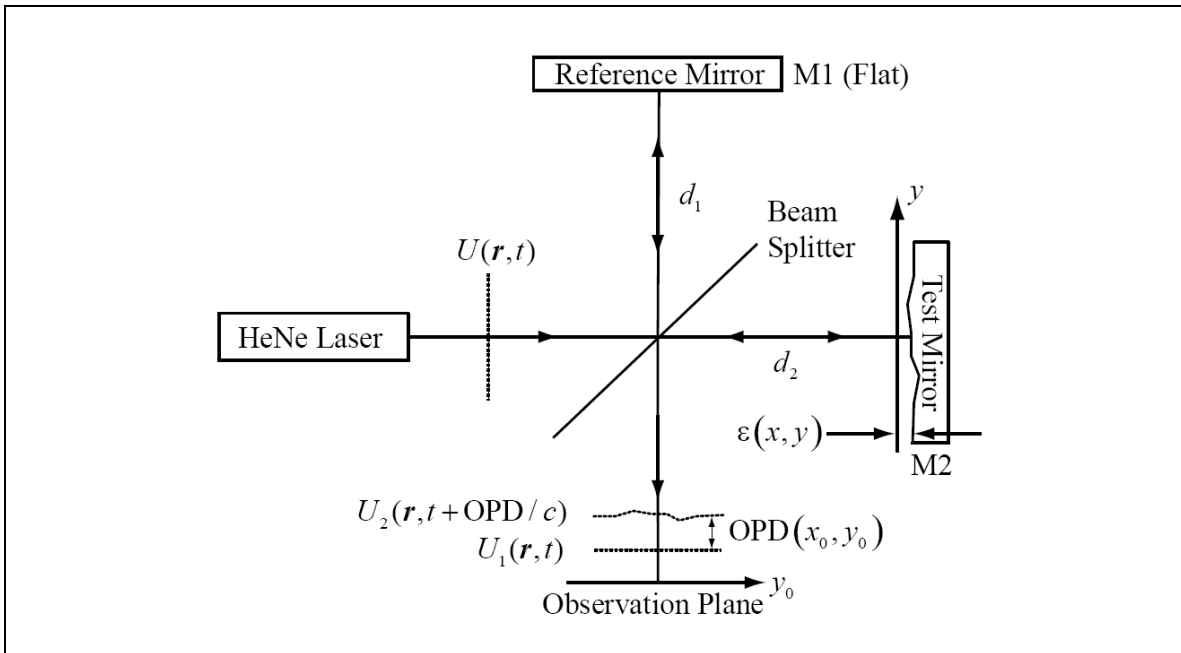


Figure 4.43. Twyman-Green Interferometer. A collimated laser beam reflects from test and reference mirrors to form the interference pattern. OPD generated from defects on the test mirror surface determines brightness of the fringe pattern.

Figure 4.44. Twyman-Green test of a spherical mirror.